

# Bayesian determination of the effect of a deep eutectic solvent on the structure of lipid monolayers

A. R. McCluskey,<sup>ab†\*</sup> A. Sanchez-Fernandez,<sup>ac‡¶</sup> K. J. Edler,<sup>a</sup>  
S. C. Parker,<sup>a</sup> A. J. Jackson,<sup>cd</sup> R. A. Campbell,<sup>ef</sup> and T. Arnold<sup>abcg\*</sup>

<sup>a</sup> Department of Chemistry, University of Bath, Claverton Down, Bath, BA2 7AY, UK.

<sup>b</sup> Diamond Light Source, Harwell Campus, Didcot, OX11 0DE, UK.

<sup>c</sup> European Spallation Source, SE-211 00 Lund, Sweden.

<sup>d</sup> Department of Physical Chemistry, Lund University, SE-211 00 Lund, Sweden.

<sup>e</sup> Institut Laue-Langevin, 71 avenue des Martyrs, 38000, Grenoble, France.

<sup>f</sup> Division of Pharmacy and Optometry, University of Manchester, Manchester, M13 9PT, UK.

<sup>g</sup> ISIS Neutron and Muon Source, Science and Technology Facilities Council, Rutherford Appleton Laboratory, Harwell Oxford, Didcot OX11 0QX, UK.

¶ Present address: Department of Food Technology, Lund University, SE-211 00 Lund, Sweden.

‡ These authors have contributed equally to the work presented within.

\* a.r.mccluskey@bath.ac.uk; tom.arnold@esss.se

## Abstract

In this work, we present the first example of the self-assembly of phospholipid monolayers at the interface between air and a non-aqueous liquid. Deep eutectic solvents are a novel class of environmentally friendly non-aqueous room temperature liquids with tunable properties, that have wide ranging potential applications and are capable of promoting the self-assembly of surfactant molecules. We use a chemically-consistent Bayesian modelling of X-ray and neutron reflectometry measurements to show that these monolayers broadly behave as they do on water. However, the ability of the deep eutectic solvent to interact with the phosphatidylglycerol lipid head, leads to an apparent increase in its volume compared to that observed in water. No such change was observed for the phosphocholine head, indicating that such interactions are head, and therefore solvent, specific. This has important implications for the potential uses of these solvents and for our understanding of how biomolecules behave in the absence of water.

Usage Electronic Supplementary Information (ESI) available: All analysis/plotting scripts and figure files, allowing for a fully reproducible, and auto-

mated, analysis workflow for the work presented is available at [https://github.com/arm61/lipids\\_at\\_airdes](https://github.com/arm61/lipids_at_airdes) (DOI: \*\*some doi\*\*) under an MIT license. Reduced experimental datasets are available at <https://researchdata.bath.ac.uk/id/eprint/548>, under a CC-BY 4.0 license.

Deep eutectic solvents (DES) are green, sustainable liquids that are obtained through the combination of ionic species with compounds that act as hydrogen bond donors, such as sugars, alcohols, amines, and carboxylic acids<sup>1,2</sup>. The resulting extensive hydrogen bonding network is able to stabilise the ionic species and allows the eutectic mixture to remain liquid at room temperature<sup>3–5</sup>. Through different combinations of the precursor materials, it is possible to tune the solvent's physicochemical properties, such as polarity<sup>6</sup>, viscosity and surface tension<sup>1</sup>, network charge<sup>7</sup>, and hydrophobicity<sup>8,9</sup>. Recently DES have also been shown to exhibit a "solvophobic" effect through the promotion of surfactant micelle formation<sup>10–13</sup>, phospholipid bilayer formation<sup>14–16</sup>, and the ability

to stabilise non-ionic polymer<sup>17</sup> and protein conformations<sup>18</sup>.

Phospholipid monolayers at the air/water interface have been widely studied as simplistic models for biological membranes. As such, they have been used to gain insight into many biological processes that are technologically and medically relevant. For example, investigations at the air/salt-water interface have identified the importance that interactions between charged phospholipid heads and ions present in solution have on the structure, monomer packing and stability of the monolayer<sup>19,20</sup>. However, the native environment for lipids in-vivo is far from a simple aqueous solution. In fact, it has been suggested<sup>2,4</sup> that DES might form within the crowded cellular environment and could assist in solubilizing biological species in an intermediate environment between that of the hydrophobic phospholipid tails and highly polar water rich regions, thereby assisting survival under extreme conditions such as freezing temperatures or drought where the water content of cells is restricted.

This work presents the first observation of phospholipid monolayers at an air-DES interface (or for that matter, any non-aqueous media, to the best of the authors' knowledge). We have used a chemically-consistent approach to model X-ray (XRR) and neutron (NR) reflectometry measurements and thereby evaluate the effect of this non-aqueous solvent on the structure of phospholipid monolayers.

Recent developments in computational resources and software have enabled powerful methodologies and algorithms to be harnessed by those from non-expert backgrounds. This has benefitted significantly from open-source software projects such as the Python language<sup>21</sup> and the Jupyter notebooks framework<sup>22</sup>. In the area of NR and XRR, the landscape of data-analysis software is diverse, with a range of software packages available from a variety of sources; *refnx*<sup>23</sup>, *MOTOFIT*<sup>24</sup>, *Rascal*<sup>25</sup> *Aurore*<sup>26</sup>, and *GenX*<sup>27</sup>.

The use of a Python library, such as *refnx*, enables the implementation custom models that contain chemically-relevant information as well as the application of probability distribution function (PDF) sampling techniques. The Python library *emcee*<sup>28</sup> offers *refnx* to access the Goodman & Weare Affine Invariant Markov chain Monte Carlo (MCMC) Ensemble method<sup>29</sup>. This allows

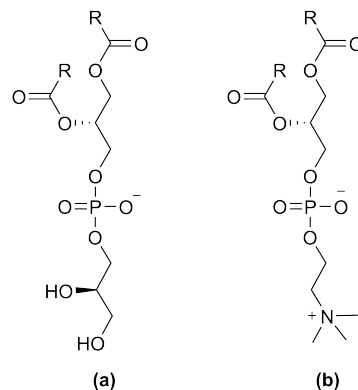


Fig. 1: The two lipid classes with different head groups compared in this study, where R indicates the hydrocarbon tail; (a) phosphatidylglycerol (PG), (b) phosphocholine (PC).

the sampling of the high-dimensionality parameter space, relevant in reflectometry analysis, in a Bayesian fashion, where the new samples are generated with consideration of those sampled previously<sup>30</sup>. Bayesian inference gives an understanding of the PDF for the fitted parameters and therefore estimations of their inverse uncertainties and inter-parameter correlations. It should be noted that these inverse uncertainties account only for the uncertainty in the analysis process and do not consider systematic uncertainties present, and unaccounted for, in the reflectometry measurement.

We report on measurements of four phospholipids monolayers, namely 1,2-dipalmitoyl-sn-glycero-3-phosphocholine (DPPC, C<sub>16</sub> tails), 1,2-dimyristoyl-sn-glycero-3-phosphocholine (DMPC, C<sub>14</sub> tails), 1,2-dilauroyl-sn-glycero-3-phosphocholine (DLPC, C<sub>12</sub> tails) and 1,2-dimyristoyl-sn-glycero-3-phospho-(1'-rac-glycerol) (DMPG, C<sub>14</sub> tails), at the air-DES (1:2 choline chloride:glycerol) interface. In contrast to many previous studies<sup>19,20,31–35</sup>, we have developed a chemically-consistent model (detail in the ESI) that allows for the co-refinement of reflectometry measurements at different surface pressure and makes no assumption of the volume of the lipid head,  $V_h$ , or tail,  $V_t$ . Instead these parameters were allowed to vary for each lipid while being constrained to be self-consistent over different surface pressures in the same phase; Liquid-Condensed (LC) for DPPC and Liquid-Expanded

(LE) for DMPC, DMPG and DLPC. This model was required because we cannot assume that the electrostatic interactions between lipid head and the solvent are the same in the DES and in water. This may therefore influence the effective head volume which means we cannot rely on the literature values (see ESI) derived from measurements on or in water. Furthermore, it is known that, on water, increased surface pressure and associated LE-LC phase transitions lead to a compression of the lipid tail volume<sup>36,37</sup> and this compaction has not necessarily been accounted for in the literature<sup>38</sup>. Our approach avoids this issue by making no assumption about the molecular volumes and only considering surface pressures that we believe to be in the same phase.

Our model has more variables than we can uniquely fit with limited data. In reflectometry the usual approach to this problem is to collect more equivalent dataset with varying deuteration (NR). For reasons of cost and practicality this was not possible in this work. The other approach is to constrain the model so that the number of fitted variables are reduced, and is the approach taken here. To do this we add the constraint that a single tail volume can be used for all surface pressures. To justify this we need to be sure that the lipids remain in the same phase. On water this can be demonstrated with a Langmuir isotherm. However, while we have confidence that the individual surface pressures measured were reliable, we were unable to collect consistent Langmuir isotherm measurements, due to the high viscosity of the DES. This inconsistency means that we cannot be confident in the phase of the lipids based on the surface pressure alone. Instead we have used grazing incidence X-ray diffraction to confirm the phases of DMPC and DPPC at 30 mNm<sup>-1</sup>. DPPC was found to be in the LC phase and DMPC in the LE phase at room temperature for the surface pressures measured (see Section S7). We assume that DMPG and DLPC are also in the LE phase since there is no reason to believe that the phase behaviour in these systems differs significantly from DMPC at the same temperature.

The model, based on the standard two-layer model widely used for lipids on water, was first fitted to the experimental XRR data. The associated SLD profiles are shown in Figure 2 while table 1 presents the results of the PDF for each of

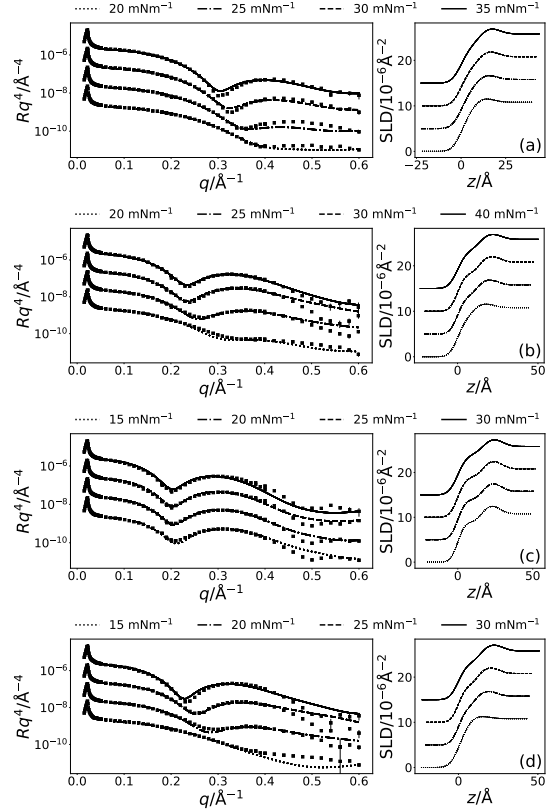


Fig. 2: The XRR profiles (left) and SLD profiles (right) for each of the four lipids; (a) DLPC, (b) DMPC, (c) DPPC, (d) DMPG, at the four measured surface pressures; see legend above each plot. The different surface pressure XRR profiles have been offset in the  $y$ -axis by an order of magnitude and SLD profiles offset in the  $y$ -axis by  $5 \times 10^{-6} \text{ \AA}^{-2}$ , for clarity.

the varying parameters; the tail tilt angle,  $\theta_t$ , the interfacial roughness,  $\sigma$ , the head and tail volumes,  $V_h$  and  $V_t$  respectively, and the head layer thickness,  $d_h$ . In order to constrain the fitting process only  $\theta_t$  and  $\sigma$  were allowed to vary independently of surface pressure. The other parameters,  $V_h$ ,  $V_t$  and  $d_h$  were fitted to a single value for all of the surface pressures measured for each lipid.

For each lipid, the tail layer thickness,  $d_t$ , increases with chain length and in general agrees with the literature for monolayers on water<sup>19,39</sup>. For DMPC,  $13.72^{+0.01}_{-0.01}$  Å at  $30 \text{ mN m}^{-1}$  in DES compared with  $d_t = 15.8$  Å at  $30 \text{ mN m}^{-1}$ <sup>32</sup> in water, and for DPPC  $16.91^{+0.01}_{-0.01}$  Å at  $30 \text{ mN m}^{-1}$  in DES compared with  $d_t = 16.7$  Å at  $40 \text{ mN m}^{-1}$ <sup>34</sup> in water. In all cases the surface roughness was found to be relatively high compared to water. This is expected because the absolute surface tension of the DES is less than water, while a previous XRR measurement of pure choline chloride:glycerol suggests a roughness of  $3.3\text{Å}$ <sup>10</sup>, significantly higher than the capillary wave roughness of water of about  $2.8\text{Å}$ .

Figure 3 shows the tail layer thickness variation with surface pressure. For DPPC and DMPC a plateau in thickness is reached at  $25 \text{ mN m}^{-1}$  and  $30 \text{ mN m}^{-1}$  respectively. Presumably a similar plateau would be seen for DMPG and DLPC at higher pressures. This phenomenon has been noted before for DMPC<sup>31</sup> and DPPC<sup>38</sup> at the air-water interface.

Figure 3 also shows that for all four lipids there is a decrease in head solvation,  $\phi_h$ , with surface pressure. This is because an increase in the surface pressure means a reduction in the free volume available between the lipid heads, which in turn forces solvent molecules out of the layer, an effect that has also been observed on water<sup>31</sup>.

Our fits suggest lower lipid tail volumes than previous measurements using other techniques (compare Tables SI and 1). It is unlikely that this is a result of the DES subphase since the tails do not directly interact with the solvent. However this may be related to the compaction of the monolayer at elevated surface pressures. The optimal value of the tail volume for DPPC in the LC phase<sup>38</sup> was found to be  $772 \text{ Å}^3$  at  $35 \text{ mN m}^{-1}$ , which agrees well with the value of  $765.32^{+0.40}_{-0.37} \text{ Å}^3$  found in this work. Similarly the tail volume for DMPS in the LE phase<sup>38</sup>,  $714 \text{ Å}^3$  at  $10 \text{ mN m}^{-1}$ , broadly agrees

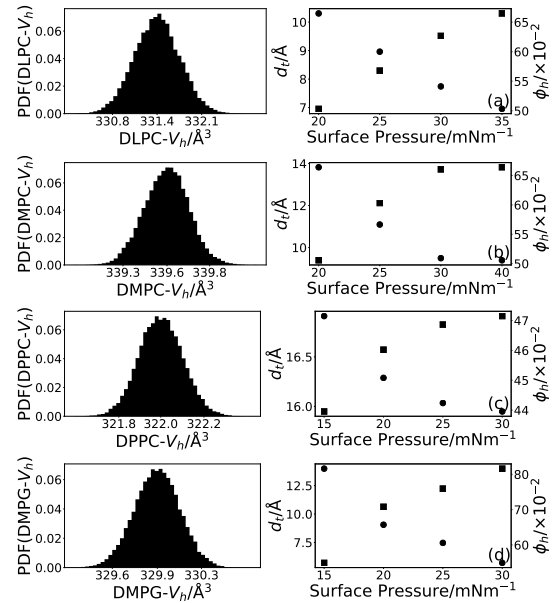


Fig. 3: The PDFs of the head volume (left) and variation of  $d_t$  (squares) and  $\phi_h$  (circles) with surface pressure for each of the four lipids; (a) DLPC, (b) DMPC, (c) DPPC, (d) DMPG. The values of  $d_t$  were found from the appropriate values of  $\theta_t$  using Eqn. S1.

Tab. 1: The best-fit values, and associated 95 % confidence intervals for the varying parameters in the XRR models, at the  $30 \text{ mN m}^{-1}$ . The values of  $d_t$  were found from the appropriate values of  $\theta_t$  using Eqn. S1 and the values for  $\phi_h$  were obtained from the appropriate use of Eqn. S3.

Lipid	DLPC	DMPC	DPPC	DMPG
$\theta_t / ^\circ$	$51.99^{+0.18}_{-0.19}$	$40.28^{+0.06}_{-0.06}$	$34.47^{+0.07}_{-0.07}$	$38.92^{+0.06}_{-0.06}$
$\sigma / \text{\AA}$	$4.16^{+0.03}_{-0.02}$	$3.86^{+0.00}_{-0.00}$	$4.90^{+0.00}_{-0.00}$	$4.44^{+0.01}_{-0.01}$
$V_t / \text{\AA}^3$	$625.21^{+3.70}_{-4.06}$	$718.75^{+0.55}_{-0.53}$	$765.32^{+0.40}_{-0.37}$	$733.99^{+0.60}_{-0.60}$
$V_h / \text{\AA}^3$	$331.43^{+0.64}_{-0.64}$	$339.55^{+0.29}_{-0.28}$	$322.00^{+0.24}_{-0.25}$	$329.94^{+0.34}_{-0.33}$
$d_h / \text{\AA}$	$10.99^{+0.13}_{-0.14}$	$13.21^{+0.04}_{-0.04}$	$12.70^{+0.03}_{-0.03}$	$13.95^{+0.03}_{-0.03}$
$\phi_h / \times 10^{-2}$	$54.12^{+1.08}_{-1.12}$	$50.93^{+0.24}_{-0.23}$	$43.96^{+0.23}_{-0.22}$	$54.91^{+0.19}_{-0.19}$
$d_t / \text{\AA}$	$9.52^{+0.04}_{-0.04}$	$13.72^{+0.01}_{-0.01}$	$16.91^{+0.01}_{-0.01}$	$13.99^{+0.01}_{-0.01}$

with the values for DMPC ( $718.75^{+0.55}_{-0.53} \text{\AA}^3$ ) and DMPG ( $733.99^{+0.60}_{-0.60} \text{\AA}^3$ ) in this work. The literature value<sup>40</sup> quoted for DMPG (at a lower temperature) is also similar to our result (but slightly smaller). We find that the reduction is 8 % to 12 % for DPPC, DMPC and DLPC when compared with literature sources at  $24^\circ\text{C}$  to  $30^\circ\text{C}$ , in good agreement with the maximum compression percentage of 15 % noted by Small *et al.*<sup>37</sup>. In general our results are at least self-consistent while comparisons to the literature are favourable.

Figure 3 shows the PDFs for the head volume for each of the four lipids. The three lipids with the PC head are consistent with values of around  $330 \text{\AA}^3$ , regardless of hydrocarbon tail. This agrees well with the values found for the same head in water (Table SI). Interestingly, the volume for the PG head is similar to that for the PC head with a value of  $329.94^{+0.34}_{-0.33} \text{\AA}^3$ , which is significantly larger than values quoted in the literature for DMPG<sup>40</sup> ( $291 \text{\AA}^3$ ) or POPG<sup>41</sup> ( $289 \text{\AA}^3$ ). This suggests that there may be some effect arising from the solvation in DES.

The major difference between the two heads is the fact PG head is negatively charged whereas the PC head is zwitterionic (Figure 1). It has been shown previously that the PC head is folded in water<sup>42</sup>, while the presence of strong electrostatic interactions in DES is known to effect the structure of surfactants micelles<sup>43</sup>. If we infer a similar folded structure for the PG head driven by a weaker interaction between the alcohol and phosphate groups, then we may explain the observed increase in volume to be due to unfolding of the PG head because we expect that the DES provides a greater charge

screening effect than water. If so then we would also expect an increase in the thickness of the head layer in DES. This does seem to be the case: The PG head layer thickness was found to be  $(10.3 \pm 0.4) \text{\AA}$  at  $22 \text{ mN m}^{-1}$ <sup>33</sup> and  $(9.7 \pm 1.0) \text{\AA}$  at  $15 \text{ mN m}^{-1}$ <sup>44</sup> from NR measurements at the air-water interface. For the PC head the stronger folding interaction, due to the formal charge on the ammonium group, means that no unfolding effect is observed.

The volumes determined for the head and tails, and the thickness of the head layers, for DMPC and DPPC were used to constrain the fitting of corresponding NR data (Figure 4). This leaves only two variables,  $\theta_t$  and  $\sigma$  to fit this data. The agreement is good and a confirmation that the volumes derived from XRR are consistent with the NR data. Furthermore, the observed trends with surface pressure are also consistent which adds some confidence in our conclusions.

For the first time, stable phosphocholine and phosphatidylglycerol lipid monolayers have been observed and characterised on a non-aqueous liquid surface. Until the emergence of ionic liquids and DES, only a limited number of molecular solvents exhibited the ability to promote self-assembly and, to the best of our knowledge, only water among those had demonstrated the formation of functional phospholipid monolayers at the air-liquid interface.

A physically and chemically constrained modelling approach and Bayesian analysis method was used to rationalise these measurements showing that the structures are remarkably similar at the air-DES interface to those previously observed at the air-water interface. This has the important implication that DES therefore offer the possibility of

Tab. 2: The best-fit values, and associated 95 % confidence intervals for the varying parameters in the co-refined NR models. The values of  $d_t$  were found from the appropriate values of  $\theta_t$  using Eqn. S1, and the values of  $\phi_h$  were found using Eqn. S3.

Lipid	d <sub>54</sub> -DMPC		d <sub>62</sub> -DPPC	
SP/mNm <sup>-1</sup>	20	25	15	20
$\theta_t/^\circ$	$38.98^{+0.75}_{-0.75}$	$24.65^{+0.06}_{-0.01}$	$53.11^{+0.45}_{-0.45}$	$40.67^{+0.42}_{-0.42}$
$\sigma_{t,h,s}/\text{\AA}$	$4.41^{+0.16}_{-0.16}$	$2.51^{+0.03}_{-0.01}$	$4.27^{+0.16}_{-0.17}$	$3.98^{+0.10}_{-0.10}$
$\phi_h/\times 10^{-2}$	$50.00^{+0.52}_{-0.53}$	$41.54^{+0.01}_{-0.03}$	$59.20^{+0.43}_{-0.43}$	$48.45^{+0.32}_{-0.32}$
$d_t/\text{\AA}$	$13.98^{+0.15}_{-0.15}$	$16.35^{+0.00}_{-0.01}$	$12.32^{+0.13}_{-0.13}$	$15.56^{+0.10}_{-0.10}$

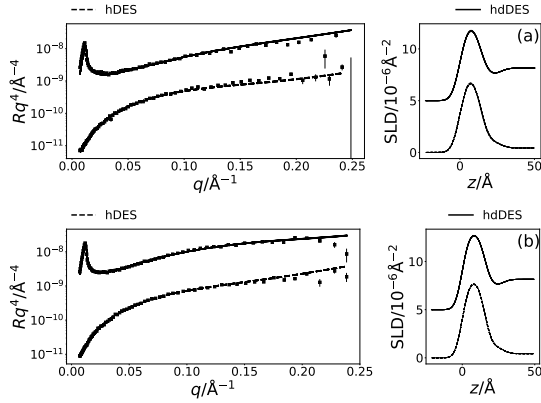


Fig. 4: The NR and SLD profiles at a surface pressure of 20 mNm<sup>-1</sup> for two contrasts (see legend above each plot); (a) DMPC, (b) DPPC. The NR profiles have been offset in the  $y$ -axis by an order of magnitude and SLD profiles offset in the  $y$ -axis by  $5 \times 10^{-6} \text{\AA}^{-2}$ , for clarity.

performing studies of model membranes in the absence of water. Such applications may include fundamental investigations of phospholipid monolayers in extreme environments (total or partial absence of water, cryogenic temperatures), protein membrane interactions and development of new technologies for drug delivery. However, the fact remains that the PG lipid did show a significant difference; having a larger head volume than observed for the same system in water. This shows that the transfer of lipids to a DES is not just a simple substitution of the subphase. In this specific case we have proposed an explanation based on unfolding of the PG head that is enabled by electrostatic screening of the head charges by the charged solvent.

The ability to determine the head volume was facilitated by access to easy to use, and open-source software that allowed for the straightforward use a custom, chemically-consistent model within the analysis of the XRR and NR measurements. Furthermore, this work presents the first, to our knowledge, use of chemically-consistent parameterisation to co-refine XRR measurements at different surface concentrations.

## Acknowledgments

The authors thank Andrew Nelson for his help with the refnx software. A.R.M. is grateful to the University of Bath and Diamond Light Source for co-funding a studentship (Studentship Number STU0149). Thanks also to the European Spallation Source and the University of Bath Alumni Fund for supporting A.S.-F. We also thank Diamond Light Source (Experiment number SI10546-1) and Institut Laue-Langevin (DOI: 10.5291/ILL-DATA.9-13-612) for the awarded beamtime.

## References

- [1] E. L. Smith, A. P. Abbott and K. S. Ryder, *Chem. Rev.*, 2014, **114**, 11060–11082.
- [2] Y. Dai, J. van Spronsen, G. J. Witkamp, R. Verpoorte and Y. H. Choi, *Anal. Chim. Acta.*, 2013, **766**, 61–68.
- [3] O. S. Hammond, D. T. Bowron and K. J. Edler, *Green Chem.*, 2016, **18**, 2736–2744.
- [4] O. S. Hammond, D. T. Bowron, A. J. Jackson, T. Arnold, A. Sanchez-Fernandez, N. Tsapataris, V. G. Sakai and K. J. Edler, *J. Phys. Chem. B*, 2017, **121**, 7473–7483.
- [5] C. F. Araujo, J. A. P. Coutinho, M. M. Nolasco, S. F. Parker, P. J. A. Ribeiro-Claro, S. Rudic, B. I. G. Soares and P. D. Vaz, *Phys. Chem. Chem. Phys.*, 2017, **19**, 17998–18009.
- [6] A. Pandey, R. Rai, M. Pal and S. Pandey, *Phys. Chem. Chem. Phys.*, 2014, **16**, 1559–1568.
- [7] S. Zahn, B. Kirchner and D. Mollenhauer, *Chem. Phys. Chem.*, 2016, **17**, 3354–3358.
- [8] B. D. Ribeiro, C. Florindo, L. C. Iff, A. Z. Coelho and I. M. Marrucho, *ACS Sustain. Chem. Eng.*, 2015, **3**, 2469–2477.
- [9] D. J. G. P. van Osch, L. F. Zubeir, A. van der Bruinhorst, M. A. A. Rocha and M. C. Kroon, *Green Chem.*, 2015, **17**, 4518–4521.
- [10] A. Sanchez-Fernandez, T. Arnold, A. J. Jackson, S. L. Fussell, R. K. Heenan, R. A. Campbell and K. J. Edler, *Phys. Chem. Chem. Phys.*, 2016, **18**, 33240–33249.
- [11] T. Arnold, A. J. Jackson, A. Sanchez-Fernandez, D. Magnone, A. E. Terry and K. J. Edler, *Langmuir*, 2015, **31**, 12894–12902.
- [12] Y.-T. Hsieh and Y.-R. Liu, *Langmuir*, 2018, **34**, 10270–10275.
- [13] M. K. Banjare, K. Behera, M. L. Satnami, S. Pandey and K. K. Ghosh, *RSC Adv.*, 2018, **8**, 7969–7979.
- [14] S. Bryant, R. Atkin and G. G. Warr, *Langmuir*, 2017, **33**, 6878–6884.
- [15] S. Bryant, R. Atkin and G. G. Warr, *Soft Matter*, 2016, **12**, 1645–1648.
- [16] M. C. Gutiérrez, M. L. Ferrer, C. R. Mateo and F. del Monte, *Langmuir*, 2009, **25**, 5509–5515.
- [17] L. Sapir, C. B. Stanley and D. Harries, *J. Phys. Chem. A*, 2016, **120**, 3253–3259.
- [18] A. Sanchez-Fernandez, K. J. Edler, T. Arnold, D. A. Venero and A. J. Jackson, *Phys. Chem. Chem. Phys.*, 2017, **19**, 8667–8670.
- [19] H. Mohwald, *Annu. Rev. Phys. Chem.*, 1990, **41**, 441–476.
- [20] S. Kewalramani, H. Hlaing, B. M. Ocko, I. Kuzmenko and M. Fukuto, *J. Phys. Chem. Lett.*, 2010, **1**, 489–495.
- [21] G. van Rossum, *Python tutorial, Technical Report CS-R9526*, Centrum voor wiskunde en informatica (cwi) technical report, 1995.
- [22] T. Kluyver, B. Ragan-Kelley, F. Pérez, B. Granger, M. Bussonnier, J. Frederic, K. Kelley, J. Hamrick, J. Grout, S. Corlay, P. Ivanov, D. Avila, S. Abdalla and C. Willing, *Positioning and Power in Academic Publishing: Players, Agents and Agendas*, 2016, pp. 87–90.
- [23] A. Nelson, S. Prescott, I. Gresham and A. R. McCluskey, *refnx v0.0.17*, 2018, <http://doi.org/10.5281/zenodo.1327191>, Available at: <http://doi.org/10.5281/zenodo.1327191>.
- [24] A. Nelson, *J. Appl. Crystallogr.*, 2006, **39**, 273–276.
- [25] A. V. Hughes, *RasCAL*, 2014, <https://sourceforge.net/projects/rscl/>, Available at: <https://sourceforge.net/projects/rscl/>.
- [26] Y. Gerelli, *J. Appl. Crystallogr.*, 2016, **49**, 330–339.
- [27] M. Björck and G. Andersson, *J. Appl. Crystallogr.*, 2007, **40**, 1174–1178.
- [28] D. Foreman-Mackey, D. W. Hogg, D. Lang and J. Goodman, *Publ. Astron. Soc. Pac.*, 2013, **125**, 306.
- [29] J. Goodman and J. Weare, *Comm. App. Math. Comp. Sci.*, 2010, **5**, 65–80.
- [30] D. S. Sivia and J. Skilling, *Data Analysis: A Bayesian Tutorial*, Oxford University Press, Oxford, UK, 2nd edn, 2006.
- [31] T. Bayerl, R. Thomas, J. Penfold, A. Rennie and E. Sackmann, *Biophys. J.*, 1990, **57**, 1095–1098.
- [32] S. J. Johnson, T. M. Bayerl, W. Weihan, H. Noack, J. Penfold, R. K. Thomas, D. Kanelas, A. R. Rennie and E. Sackmann, *Biophys. J.*, 1991, **60**, 1017–1025.

- 
- [33] L. A. Clifton, M. Sanders, C. Kinane, T. Arnold, K. J. Edler, C. Neylon, R. J. Green and R. A. Frazier, *Phys. Chem. Chem. Phys.*, 2012, **14**, 13569–13579.
- [34] C. A. Helm, H. Möhwald, K. Kjær and J. Als-Nielsen, *EPL*, 1987, **4**, 697.
- [35] J. Daillant, L. Bosio and J. J. Benattar, *EPL*, 1990, **12**, 715.
- [36] D. Marsh, *Chem. Phys. Lipids*, 2010, **163**, 667–677.
- [37] D. M. Small, *J. Lipid Res.*, 1984, **25**, 1490–1500.
- [38] R. A. Campbell, Y. Saaka, Y. Shao, Y. Gerelli, R. Cubitt, E. Nazaruk, D. Matyszevska and M. J. Lawrence, *J. Colloid Interface Sci.*, 2018, **531**, 98–108.
- [39] D. Vaknin, K. Kjaer, J. Als-Nielsen and M. Lösche, *Biophys. J.*, 1991, **59**, 1325–1332.
- [40] J. Pan, F. A. Heberle, S. Tristram-Nagle, M. Szymanski, M. Koepfinger, J. Katsaras and N. Kučerka, *BBA - Biomembranes*, 2012, **1818**, 2135–2148.
- [41] N. Kučerka, B. W. Holland, C. G. Gray, B. Tomberli and J. Katsaras, *J. Phys. Chem. B*, 2012, **116**, 232–232.
- [42] R. J. Gillams, C. D. Lorenz and S. E. McLain, *J. Chem. Phys.*, 2016, **144**, 225101.
- [43] A. Sanchez-Fernandez, G. L. Moody, L. C. Murfin, T. Arnold, A. J. Jackson, S. M. King, S. E. Lewis and K. J. Edler, *Soft Matter*, 2018, **14**, 5525–5536.
- [44] D. Ciumac, R. A. Campbell, H. Xu, L. A. Clifton, A. V. Hughes, R. P. Webster, J. and J. R. Lu, *Colloids Surf. B*, 2017, **150**, 308–316.